A comparative study between inner and outer rotor variable flux reluctance machine topologies for heavy-duty electric vehicles

A Comparative Study between Inner and Outer Rotor Variable Flux Reluctance Machine Topologies For Heavy-duty Electric Vehicles

Doğa Ceylan, Konstantin O. Boynov, Elena A. Lomonova

Department of Electrical Engineering, Eindhoven University of Technology, 5612 Eindhoven, The Netherlands
d.ceylan@tue.nl

Keywords: Variable flux reluctance machine, outer and inner rotor, optimal design, heavy-duty electric vehicles.

Abstract

This article presents a comprehensive comparative study between two variable flux reluctance machine topologies with inner and outer rotors. Electrical and geometrical parameters of both topologies are optimized for maximum torque density, minimum torque ripple, and maximum efficiency to be used in a heavy-duty electric vehicle which requires 500 Nm electromagnetic torque at 1200 rpm base speed. Then, both optimal designs are compared using the 2-D and 3-D finite element and analytical models. The 2-D electromagnetic finite element model coupled with a 3-D analytical thermal model shows that the outer rotor VFRM is able to reach higher torque density with 21 Nm/L than inner rotor topology when the water cooling is also included in the volume of the electrical machine. Although the optimal variable flux reluctance machine with the inner rotor exhibits slightly lower efficiency and higher torque ripple than the optimal design with the outer rotor, it is possible to apply higher current densities with the outer rotor topology due to its improved thermal characteristics. However, the 3-D mechanical finite element model coupled with the electromagnetic model shows that the maximum von Mises stress and deformation in the electrical steel is more than one order of magnitude higher in the outer rotor topology than the inner rotor topology.

1 Introduction

The variable flux reluctance machine (VFRM) [1] is considered as an alternative to the permanent-magnet (PM) synchronous machine by many researchers and engineers from the field of electromechanics since its PM-free structure reduces the cost of the electrical machine and eliminates the risk of demagnetization of PMs. In addition to its robust and cost-effective structure, VFRM exhibits double saliency while it has electrical excitation only in its stator. Therefore, the heat sources are located only in its stator while the PM synchronous machine dissipates the heat in both its stator and rotor. Moreover, VFRM demonstrates higher efficiency than other reluctance machines such as the doubly-fed doubly salient machine beyond the base speed, since it implements the flux weakening by reducing the dc-field current instead of producing a negative direct axis current [2]. Although its operation principle is similar to the switch reluctance machine, VFRM exposes less acoustic noise due to its sinusoidal flux linkage and back electromotive force [3]. Particularly, it is shown that the torque ripple of VFRM can be reduced by rotor skewing [4], rotor shaping [5], or harmonic field current injection [6].

Besides its aforementioned advantages, VFRM should be optimally designed to be competitive with the PM synchronous machine in torque density and efficiency. In [7], a VFRM with an inner rotor is optimized for the nominal operating point, which is 150 Nm and 4800 rpm, using the block coordinate descent optimization method. Also, the rotor pole arc of an inner rotor VFRM is optimized in [8] to maximize the torque production where the average torque is less than 1 Nm. Although there exist a few studies in the literature on the optimal design of VFRM, it is not fully investigated for applications requiring a large electromagnetic torque generation such as heavy-duty electric vehicles. High torque requirement increases the amount of the PM material used in PM synchronous machines and thereby the total cost. For instance, a rare-earth-free PM-assisted synchronous reluctance machine with 450 Nm continuous peak torque and 2800 rpm base speed is designed for heavy-duty electric vehicles in [9], since the use of rare-earth magnets fails to meet the low-cost requirements.

In this study, the PM-free VFRM is investigated to be used in the traction of a heavy-duty electric vehicle. While the maximum continuous torque of the electrical machine is 500 Nm, the base rotor speed where the flux weakening region starts is found to be 1200 rpm considering the selected 1:120 gearbox ratio. Two topology options are compared: inner and outer rotor VFRMs for satisfying the same machine requirements. Firstly, geometric and electrical parameters of both topologies are optimized to meet design requirements with maximum torque density, maximum efficiency and minimum torque ripple. Then, the electromagnetic, thermal, and mechanical aspects of both optimized VFRMs are compared to select the most suitable one for the heavy-duty electric vehicle application.

2. Optimization methodology

Before starting the optimization, some of the design parameters are selected considering the available literature and initial sizing study. For instance, [10] shows that an odd number of rotor poles results in an unbalanced magnetic pull and therefore increases the vibration in VFRMs. Also, the

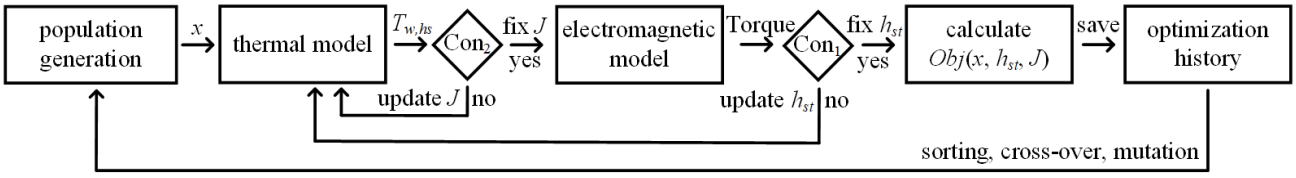

Fig. 1: Optimization flowchart.

12/10 stator/rotor pole combination is found to be advantageous among the other combinations with an even number of rotor poles for having more sinusoidal flux linkage and higher torque density. Therefore, the stator/rotor pole combination is fixed to 12/10 respectively in the optimization for both inner and outer rotor topologies. In addition, double-layer concentrated windings are used in the optimization of both topologies, since they exhibit higher average torque, less torque ripple, less iron loss, and higher efficiency than the single-layer structure [11]. In order to decide the maximum and minimum values of the geometric optimization parameters, an initial sizing study is conducted by radial scaling of an available inner rotor VFRM designed in [12]. This VFRM is scaled in the radial direction using a 2-D nonlinear magnetostatic finite element method (FEM) until it is able to generate the required average torque. The machine aspect ratio, which is the ratio of the machine outer diameter to the stack length, is selected as 0.5 for the initial sizing study, since the pancake type structure with an aspect ratio larger than unity increases the end winding effects. As the result of the initial sizing study, the limits of the radial geometric parameters are decided while the stack length of both types of VFRM is selected as 500 mm. Furthermore, the air gap is fixed to 1 mm for both inner and outer rotor topologies, since the manufacturing tolerances may cause non-uniform airgap for electrical machines with less than 1 mm air gap. The shaft diameter is fixed to 40 mm which results in 39 MPa maximum shear stress according to (1).

$$\tau_{max} = \frac{16T}{\pi D^3} \tag{1}$$

In (1), τ_{max} is the maximum shear stress generated on the shaft outer surface, T is the maximum torque applied to the shaft, and D is the shaft diameter. NO27 is selected as the material of the electrical steel domains. Finally, the water cooling is selected as the active cooling type to increase the maximum applicable current density, where the root-mean-square (rms) value of the ac current density is taken equal to the dc current density. The aforementioned parameters are kept constant as explained while eight optimization variables are selected to define the geometry and electrical excitation of both inner and outer rotor topologies. These variables are rotor tooth opening angle on the rotor yoke side (θ_{ry}), rotor tooth opening angle on the air gap side (θ_{ra}), stator tooth opening angle on the stator yoke side (θ_{sy}), stator tooth opening angle on the air gap side (θ_{sa}), rotor yoke height (h_{ry}), rotor tooth height (h_{rt}), stator yoke height (h_{sy}), ratio of ac excitation height to dc excitation height in the stator slot (h_{ac}/h_{dc}). Lower and upper boundaries of listed optimization variables are decided considering results of the initial sizing study such a way that the defined boundaries do not result in any error in the geometry generation. Defined geometric variables are optimized using the genetic algorithm of the MATLAB optimization toolbox. A 2-D nonlinear magnetostatic FEM model is developed using COMSOL Multiphysics to solve the electromagnetic problem of both inner and outer rotor topologies. The developed FEM model is called by the genetic algorithm using COMSOL LiveLink for each individual defined in (2) to calculate its objective function, $Obj(x)$, which includes three components as in (3).

$$x = \left[\theta_{ry}, \theta_{ra}, \theta_{sy}, \theta_{sa}, h_{ry}, h_{rt}, h_{sy}, \frac{h_{ac}}{h_{dc}}\right] \tag{2}$$

$$Obj(x) = w_1 \frac{T_{ave}}{V} + w_2 \eta - w_3 \frac{T_{max} - T_{min}}{T_{ave}} \tag{3}$$

In the objective definition, T is the developed electromagnetic torque, V is the total volume of the VFRM, η is the efficiency, T_{max}, T_{min}, and T_{ave} are the maximum, minimum, and average value of the torque in one electrical period. Additionally, w_1, w_2, and w_3 are weight coefficients selected as $25^{-1}, 0.85^{-1}, 0.1^{-1}$, which are one over the estimated values for the torque density in Nm/L, the efficiency, and the ratio of torque ripple to the average torque, to reduce the effect of the unit difference between three components. Moreover, the height of the stator slot in the radial direction and the applied current density are calculated using two defined constraints as in (4).

$$\begin{aligned} &\text{maximize} && Obj(x) \\ &\text{subject to} && \text{Con}_1\text{: } 480 \text{ Nm} < T_{ave}(x) < 520 \text{ Nm}, \\ & && \text{Con}_2\text{: } 90^0\text{C} < T_{w,hs}(x) < 100^0\text{C} \end{aligned} \tag{4}$$

T_{ave} of Con$_1$ (constraint 1) is the average electromagnetic torque, $T_{w,hs}$ of Con$_2$ (constraint 2) is the temperature of the hottest spot in the windings. The constraint on the average torque is satisfied by selecting a proper stator slot height (also called stator tooth height, h_{st}) using the 2-D nonlinear electromagnetic FEM model while the constraint on the winding temperature is satisfied by selecting a proper current density (J) using a 3-D analytical steady-state thermal model. The optimization study is carried for the nominal operating point where the torque is 500 Nm and speed is 1200 rpm. The optimization flowchart is illustrated in Fig. 1. Individuals of a generation, x in (2), are taken as the input by the thermal model to satisfy Con$_2$. Then, the calculated J is used by the electromagnetic model with x to find an appropriate h_{st}. After fixing J and h_{st}, the objective is calculated using (3). Finally, the stochastic, population-based genetic algorithm creates the

new generation randomly by mutation and cross-over among population members.

3. Results

3.1 Optimal designs

Geometric and electrical parameters of VFRMs with inner and outer rotors are optimized to maximize the described objective function. The resultant angular and radial geometric parameters defining the motor geometry and excitation are listed in Table 1 and Table 2, respectively. Moreover, the maximum current densities which satisfy both Con_1 and Con_2 for the optimum inner and outer rotor topologies are found to be 9.1 and 12.5 A/mm^2, respectively. Although the current density of the dc-field windings and rms current density of the ac-field windings are selected the same, different coil areas of ac and dc coils in one slot cause different dc and rms-ac current levels.

Table 1: Optimal values of the angular parameters.

rotor type	θ_{ry} [deg]	θ_{ra} [deg]	θ_{sy} [deg]	θ_{sa} [deg]
inner:	26	12	13	14
outer:	21	15	21	12

Table 2: Optimal values of the radial parameters.

rotor type	h_{ry} [mm]	h_{rt} [mm]	h_{sy} [mm]	$\frac{A_{ac}}{A_{dc}}$ [-]	h_{st} [mm]
inner:	37	29	13	1.2	29
outer:	12	8	16	1.1	27

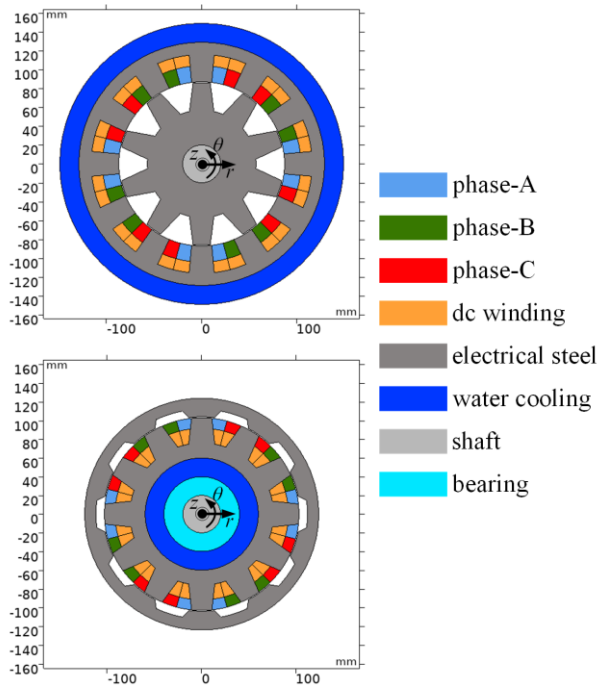

Fig. 2: Optimal geometries of the VFRMs with inner (upper) and outer (lower) rotors.

Additionally, cross-sectional views of optimum geometries are illustrated with actual dimensions in Fig. 2. The defined active water cooling is placed outside of the stator for the inner rotor, while it is placed inside of the stator for the outer rotor topology. The diameter of water cooling channels is chosen as 20 mm in both cases. Moreover, a bearing has to be located between the shaft and stator of the outer rotor topology since the rotating shaft is connected to the rotor from one end-side of the outer rotor topology while the stationary stator is fixed to the frame from the other end-side. The length of the defined bearing is selected as 20 mm in the radial direction. Electromagnetic, thermal, and mechanical performances of the optimal designs are investigated using the developed FEM and analytical models.

3.2 Electromagnetic aspects

A 2-D magnetostatic FEM model is used to calculate the magnetic flux density distribution inside both topologies for different rotor positions. The nonlinear single-valued magnetic saturation curve of NO27 electrical steel is defined in iron domains. The current excitation is assigned for both ac- and dc-field copper windings. Time independent differential form of the vector potential formulation (5) and (6), so called Ampère's law is employed with the magnetic flux conservation (7).

$$\nabla \times H = J \tag{5}$$

$$B = \nabla \times A \tag{6}$$

$$\nabla \cdot B = 0 \tag{7}$$

In the used magnetostatic formulation, H is the magnetic field strength, B is the magnetic flux density, and A is the magnetic vector potential. In addition, the Dirichlet boundary condition is defined at the outer boundaries of both topologies ignoring the leakage flux. High frequency effects such as the magnetic hysteresis, eddy currents are neglected in the used electromagnetic model due to a relatively low excitation frequency, 200 Hz. The normalized magnetic flux density distributions of both optimized topologies for the initial rotor position are presented in Fig. 3.

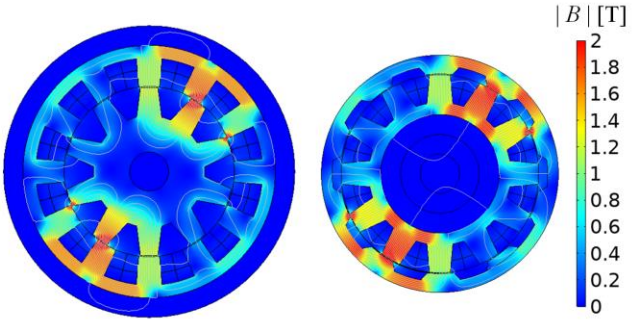

Fig. 3: The magnetic flux density distribution of inner rotor (left) and outer rotor (right) topologies.

The electromagnetic torque is calculated using the flux density found in Fig. 3 and Arkkio's torque calculation method as in (8), where r_1 is the rotor radius for the inner rotor topology and the stator radius for the outer rotor topology, l_s is the stack length which is 500 mm, B_r is the magnetic flux density in the

radial direction, B_θ is the magnetic flux density in the angular direction, μ_0 is the permeability of vacuum which is $4\pi 10^{-7}$ H/m, and δ is the air gap distance which is 1 mm.

$$T = \int_{r_1}^{r_1+\delta} \int_0^{2\pi} \frac{r l_s B_r B_\theta}{\mu_0 \delta} d\theta dr \qquad (8)$$

The torque is calculated for 100 rotor positions for one electrical period and the generated torque waveforms of both VFRM topologies are compared in Fig. 4(a). Furthermore, the total number of turns of each phase is selected as 56 and 48 for inner and outer rotor topologies to keep the peak value the phase voltage less than 400 V. Therefore, the total flux linkage of phase-A is similar for both inner and outer topologies as in Fig 4(b). Moreover, the selected numbers of turns of ac-field windings provides 90 and 98 A rms phase currents for inner and outer rotor topologies, respectively.

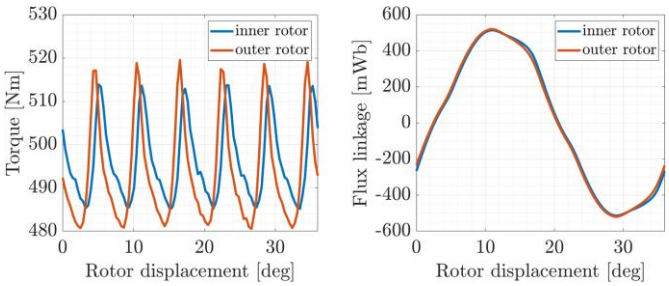

(a) (b)

Fig. 4: Torque generation (a) and flux linkage of phase-A (b) of inner and outer rotor VFRM topologies.

Table 3: Objectives of the optimum designs.

rotor type	$\frac{T_{ave}}{V}$	η	$\frac{T_{max}-T_{min}}{T_{ave}}$
inner:	14 Nm/L	84%	6%
outer:	21 Nm/L	81%	8%

The described electromagnetic model is also used in the optimization to calculate (3) for the rated torque at the base speed. The efficiency is calculated using the output power which is torque times speed, the copper loss of ac- and dc-field windings, the friction loss at the bearings which is estimated as 60 W and the iron loss. For the calculation of iron loss, the statistical loss separation theory of Bertotti is employed. It is based on the decomposition of the eddy current, hysteresis, and excess loss assuming that the flux density waveforms are sinusoidal and the excitation frequency is up to and including 300 Hz. Values of the pareto front objective components defined in (3) are presented in Table 3 for both inner and outer rotor topologies.

3.3 Thermal aspects

A 3-D analytical steady-state thermal model is developed to compare inner and outer rotor VFRMs and to be used in the optimization of both electrical machines. The equivalent thermal network used for both inner and outer rotor VFRMs is illustrated in Fig. 5, where the values of the thermal resistances differs for both topologies. In Fig. 5, five loss components are defined as heat sources: the copper loss in windings (P_{cu}), the iron loss in the stator and the rotor ($P_{fe,s}$, $P_{fe,r}$), the mechanical loss in bearings (P_{fw}). The proposed equivalent circuit is employed to calculate temperatures of six domains: the outer surface of windings ($T_{w,os}$), the hottest spot inside windings ($T_{w,hs}$), the stator (T_s), the rotor (T_r), bearings (T_b), and the frame (T_f), where T_a is the ambient temperature. Moreover, resistors defined in Fig. 5 are named considering the domains that they connect, for instance R_{sr} is the thermal resistance between the stator and rotor. Note R_{sa} is calculated considering the water cooling inside the stator of the outer rotor topology, while it is taken as infinity for the inner rotor topology since there is no heat transfer from the stator to ambient in this topology. R_{wf}, R_{rf}, R_{rs}, and R_{fa} are calculated using their the convective heat transfer coefficient based on empirical equations while the rest of thermal resistances spread the heat by conduction. Calculation of each thermal resistance will be discussed in the full paper. Finally, the change in the maximum winding temperature with respect to the current density is compared for both topologies in Fig. 6.

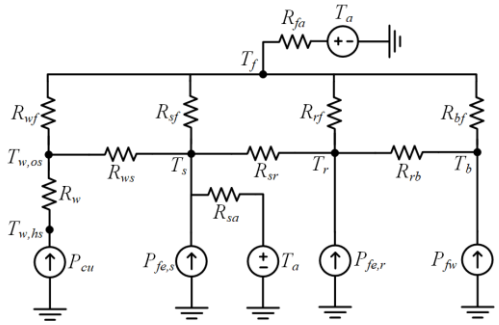

Fig. 5: Equivalent thermal network of VFRMs.

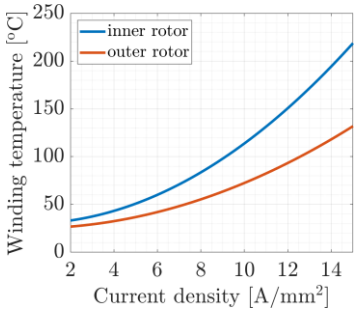

Fig. 6: Maximum temperature inside the winding of optimum inner and outer rotor VFRM designs with respect to the current density.

3.4 Mechanical aspects

To investigate the mechanical aspects of both topologies, the electromagnetic model should be coupled with a mechanical model. Although 2-D modeling is sufficient for the inner rotor topology, a 3-D model is required for the outer rotor one since the rotor is fixed to the shaft from one end of the motor. Therefore, 3-D coupled FEM models are developed and the analyzed geometries are presented in Fig. 7. The same current densities calculated by the thermal model are applied for the initial rotor position. The mechanical model takes the Maxwell

stress tensor values on the interfaces between stator/airgap and rotor/airgap as input. In the mechanical model, two sides of the shaft and the bottom surface of the motor frame are defined as the fixed constraint meaning that the displacement is zero while the rotor, the stator, and the rest of the shaft and frame are defined as free to get deformed depending on the material Young's modulus. Poisson's ratio, and density. The von Mises stress and the deformation are calculated and presented in Fig. 8 and Fig. 9, respectively. The results show that the outer rotor topology suffers from the mechanical stress acting on its rotor and the resultant displacement changes its air gap by 10%, while the deformation in the inner rotor topology is negligible.

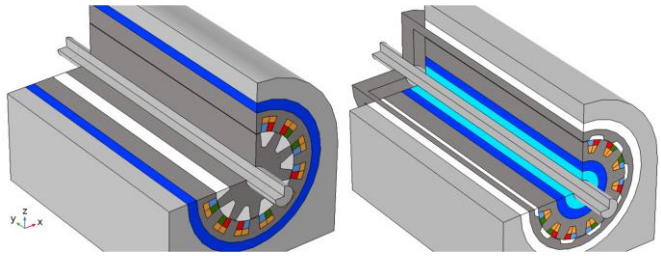

(a) (b)

Fig. 7: Geometries of the 3-D mechanical model for both inner (a) and outer rotor (b) topologies.

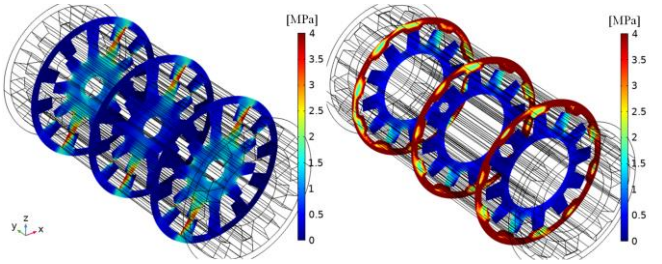

(a) (b)

Fig. 8: Distribution of the magnitude of the von Mises stress in both inner (a) and outer rotor (b) topologies.

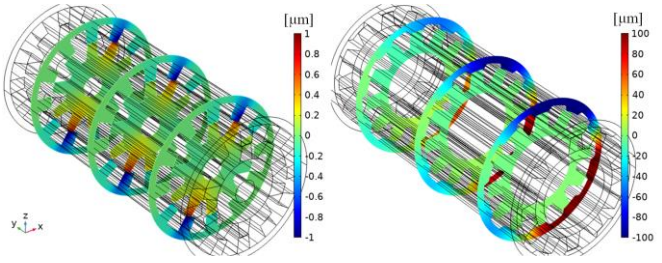

(a) (b)

Fig. 9: Deformation distribution of the rotor and stator in the radial direction for inner (a) and outer rotor (b) topologies.

4 Conclusion

The outer and inner rotor VFRM topologies are optimized and later the optimal designs are compared considering their electromagnetic, thermal, and mechanical performances. Although the outer rotor topology is superior for a higher torque density due to its improved thermal characteristics, the high mechanical stress on its rotor causes a non-uniform air gap which affects its torque production. Therefore, it is concluded that mechanical stress should be included in the optimization of the outer rotor topology. Moreover, the deformation in the outer rotor topology could be decreased by decreasing the stack length of the motor. Hence, the stack length could be also included in the optimization.

5 References

[1] Liu, X., Zhu, Z. Q.: 'Electromagnetic performance of novel variable flux reluctance machines with dc-field coil in stator', IEEE Trans. Magn., 2013, 49, (6), pp. 3020–3028

[2] Liu, X., Zhu, Z. Q.: 'Design and investigation of flux weakening capability in VFRMs. Proc. IEEE Vehicle Power and Propulsion Conf., Hangzhou, China, Oct. 2016, pp. 1–6

[3] Liu, X., Zhu, Z. Q.: 'Comparative study of novel variable flux reluctance machines with doubly fed doubly salient machines', IEEE Trans. Magn., 2013, 49, (7), pp. 3838–3841

[4] Bao, J., Gysen, B. L. J., Boynov K. O., et al.: 'Torque ripple reduction for 12-staqtor 10-rotor-pole variable flux reluctance machines by rotor skewing or rotor teeth non-uniformity', IEEE Trans. Magn., 2017, 53, (11), pp. 1–5

[5] Huang, L. R., Feng, J. H., Guo S. Y., et al.: 'Rotor shaping method for torque ripple mitigation in VFRMs, IEEE Trans. Energy Convers, 2018, 33, (3), pp. 1579–1589

[6] Lee, B., Zhu, Z. Q., Huang L. R.: 'Torque ripple reduction for 6-stator/4-rotor-pole variable flux reluctance machine by using harmonic field current injection', IEEE Trans. Ind. App., 2017, 53, (4), pp. 3730–3737

[7] Zuurbier, M. M. J., Fahdzyana, C. A., Hofman, T., et al.: 'Geometric optimization of variable flux reluctance machines for full electric vehicles'. Proc. Int. Conf. on Ecological Vehicles and Renewable Energies, Monte-Carlo, Monaco, May. 2019, pp. 1–9

[8] Dexter, J., Huang, L., Zhu, Z. Q., et al.: 'Comparison of torque production and design of switch reluctance and variable flux reluctance machines'. Proc. Int. Conf. on Electrical Machines and Systems, Jeju, Korea, Oct. 2018, pp. 1–6

[9] Al-ani, M., Rocca, S. L., Rocca, A. L., et al.: 'Design of rare-earth-free PM-assisted synchronous reluctance machine for heavy-duty automotive applications'. Proc. Int. Conf. on Power Elect., Mach. and Drives, Online, Dec. 2020, pp. 1–7

[10] Shi, J. T., Zhu, Z. Q.: 'Analysis of novel multi-tooth VFRMs with different stator and rotor pole combinations', IEEE Trans. Magn., 2015, 51, (5), pp. 1–11

[11] Huang, L., Zhu, Z. Q., Feng, J.: 'Comparative analysis of variable flux reluctance machines with double- and single-layer concentrated armature windings', IEEE Trans. Ind. Appl., 2019, 55, (2), pp. 1505–1515

[12] Bao, J.: 'Hybrid modeling technique for nonlinear 2D electromagnetic problems: towards a design framework for variable flux reluctance machines'. PhD thesis, Eindhoven University of Technology, 2019